Quadrotor Accelerometer and Gyroscope Sensor Fault Diagnosis with Experimental Results

Remus C Avram[1],*, Xiaodong Zhang[2] and Jonathan Muse[3†]

[1,2] *Wright State University, Dayton, Ohio, 45404, USA*
avram.3@wright.edu
xiaodong.zhang@wright.edu

[3] *Air Force Research Laboratory, Dayton, OH, 45433, USA*
jonathan.muse.2@us.af.mil

ABSTRACT

This paper presents the design and real-time experimental results of a fault diagnosis scheme for inertial measurement unit (IMU) measurements of quadrotor unmanned air vehicles (UAVs). The objective is to detect, isolate, and estimate sensor bias fault in accelerometer and gyroscope measurements. Based on the quadrotor dynamics and sensor models under consideration, the effects of sensor faults are represented as virtual actuator faults in the quadrotor state equations. Two nonlinear diagnostic estimators are designed to provide structured residuals enabling the simultaneous detection and isolation of the sensor faults. Additionally, based on the detection and isolation scheme, two nonlinear adaptive estimators are employed for the estimation of the fault magnitude. The performance of the diagnosis method is evaluated and demonstrated through real-time flight experiments.

1. INTRODUCTION

Unmanned Aerial Vehicles (UAVs) have attracted significant attentions in recent years due to their potentials in various military and civilian applications, including security patrol, search and rescue in hazardous environment, surveillance and classification, attack and rendezvous (Shima & Rasmussen, 2008). Most quadrotors used in research, are often equipped with low-cost and lightweight micro-electro-mechanical systems (MEMS) inertial measurement units (IMU) including 3-axis gyro, accelerometer and magnetometer. These sensors serve an essential role in most quadrotor control schemes. However, due to their intrinsic components and fabrication process, IMUs are vulnerable to exogenous signals and prone to faults. Specifically, accelerometer and gyroscope measurements are susceptible to bias and excessive noise as a result of temperature variation, vibration, etc. The detection and estimation of accelerometer and gyroscope faults plays a crucial role in the safe operations of quadrotors. In this paper we present a nonlinear method for detecting, isolating and estimating sensor bias faults in accelerometer and gyroscope measurements of quadrotor UAVs. Based on the fact that the accelerometer and the gyroscope measure forces/torque acting directly on the UAV body, the quadrotor dynamics are expressed in terms of the IMU sensor measurements. Two robust diagnostic estimators are designed to provide structured fault detection and isolation (FDI) residuals allowing simultaneous detection and isolation of gyroscope and accelerometer sensor bias in the presence of measurement noise. In addition, by utilizing nonlinear adaptive estimation techniques (Zhang, Polycarpou, & Parsini, 2001), adaptive estimators are employed to provide an estimate of the unknown sensor bias. The parameter convergence property of the adaptive estimation scheme is analyzed.

The remainder of the paper is organized as follows. Section 2 formulates the problem of sensor FDI for quadrotor UAVs. The proposed fault detection and isolation method is presented in Section 3. Section 4 describes the adaptive estimator algorithms for estimating the unknown sensor bias magnitude and provides conditions for parameter convergence. Section 5 and 6 present experimental results and direction of future research, respectively.

2. PROBLEM FORMULATION

As in (Leishman, Jr., Beard, & McLain, 2014) and (Martin & Salaün, 2010), the dynamic model used in this paper considers the gravity, thrust generated by the rotors and drag forces acting on the quadrotor body. The quadrotor nominal system dynamics are derived from the Newton-Euler equations

†Distribution Statement A, Approved for Public Release; Distribution Unlimited. Cleared by 88 ABW/PA, 22 JUL 2015 (88ABW-2015-3703)

of motion and are given by:

$$\dot{p}_E = v_E \tag{1}$$

$$\dot{v}_E = \frac{1}{m} R_{EB}(\eta) \left(\begin{bmatrix} 0 \\ 0 \\ -U \end{bmatrix} - c_{\mathbf{d}} v_B \right) + \begin{bmatrix} 0 \\ 0 \\ g \end{bmatrix} \tag{2}$$

$$\dot{\eta} = \begin{bmatrix} 1 & \sin\phi\tan\theta & \cos\phi\tan\theta \\ 0 & \cos\phi & -\sin\phi \\ 0 & \sin\phi\sec\theta & \cos\phi\sec\theta \end{bmatrix} \omega \tag{3}$$

$$\begin{bmatrix} \dot{p} \\ \dot{q} \\ \dot{r} \end{bmatrix} = \begin{bmatrix} \frac{J_y - J_z}{J_x} qr \\ \frac{J_z - J_x}{J_y} pr \\ \frac{J_x - J_y}{J_z} pq \end{bmatrix} + \begin{bmatrix} \frac{1}{J_x}\tau_\phi \\ \frac{1}{J_y}\tau_\theta \\ \frac{1}{J_z}\tau_\psi \end{bmatrix} \tag{4}$$

where $p_E \in \mathbb{R}^3$ is the inertial position, $v_E \in \mathbb{R}^3$ is the velocity expressed in the Earth frame, $\eta = [\phi,\, \theta,\, \psi]^T \in \mathbb{R}^3$ are the roll, pitch and yaw Euler angles, respectively, and $\omega = [p\,, q\,, r]^T$ represents the angular rates, m is the mass of the quadrotor, and g is the gravitational acceleration. The terms J_x, J_y and J_z represent the quadrotor inertias about the body x-, y- and z-axis, respectively. Note that the quadrotor is assumed to be symmetric about the xz and yz planes (i.e. the product of inertias is zero). U represents the total thrust generated by the rotors, τ_ϕ, τ_θ, τ_ψ are the torques acting on the quadrotor around the body x-, y- and z-axis, respectively. The term $c_{\mathbf{d}} v_B$ represents the drag force acting on the vehicle frame, with $c_{\mathbf{d}}$ being drag force coefficient and v_B is the velocity of the UAV relative to the body frame.

The system model described by Eq (1) - (4) is expressed with the velocity relative to the inertial frame. The inertial coordinate system is assumed to have the positive x-axis pointing North, the positive y-axis pointing East and positive z-axis pointing down towards the Earth's center. The transformation from the body frame to inertial frame is given by the rotation matrix R_{EB} and is defined based on a 3-2-1 rotation sequence as follows:

$$R_{EB}(\eta) = \begin{bmatrix} c\theta c\psi & s\phi s\theta c\psi - c\phi s\psi & c\phi s\theta c\psi + s\phi s\psi \\ c\theta s\psi & s\phi s\theta s\psi + c\phi c\psi & c\phi s\theta s\psi - s\phi c\psi \\ -s\theta & s\phi c\theta & c\phi c\theta \end{bmatrix}$$

where $s\cdot$ and $c\cdot$ are short hand notations for the $\sin(\cdot)$ and $\cos(\cdot)$ functions, respectively. As in (Leishman et al., 2014), by assuming that the nonlinear Coriolis terms are small enough to be negligible, the quadrotor velocity dynamics relative to the body frame are expressed as

$$\begin{bmatrix} \dot{u} \\ \dot{v} \\ \dot{w} \end{bmatrix} = \frac{1}{m} \left(\begin{bmatrix} 0 \\ 0 \\ -T \end{bmatrix} - c_{\mathbf{d}} v_B \right) + \begin{bmatrix} -g\sin\theta \\ g\sin\phi\cos\theta \\ g\cos\phi\cos\theta \end{bmatrix} \tag{5}$$

where $v_B = [u,\, v,\, w]^T$, represents the velocities along the body $x-$, $y-$ and $z-$direction. The relation between the inertial velocity and body velocity is given by $v_E = R_{EB} v_B$.

As in (Ireland & Anderson, 2012) and (Lantos & Marton, 2011), it is assumed that Euler angles measurements are available. For instance, these measurements can be generated by a camera-based motion capture system, a technology commonly employed for in-door UAV flight (Guenard, Hamel, & Mahony, 2008).

MEMS sensors, such as accelerometers and gyroscopes, measure forces and moments acting in the body frame. The quantity expressed inside the parenthesis in the inertial velocity dynamics described by Eq (2), represents all the forces acting on the body. Therefore, the inertial velocity dynamic equation can be adjusted to reflect accelerometer measurements. Similarly, the evolution of Euler angles can be rewritten in terms of gyroscope measurements. By considering IMU measurement's susceptibility to bias faults, the accelerometer and gyroscope sensor measurements are given by:

$$\begin{aligned} y_a &= a + b_a + d_a \\ &= \frac{1}{m} \left(\begin{bmatrix} 0 \\ 0 \\ -U \end{bmatrix} - c_{\mathbf{d}} v_B \right) + \beta_a(t - T_a) b_a + d_a \end{aligned} \tag{6}$$

$$y_\omega = \omega + b_\omega + d_\omega = \begin{bmatrix} p \\ q \\ r \end{bmatrix} + \beta_\omega(t - T_\omega) b_\omega + d_\omega \tag{7}$$

where $y_a \in \mathbb{R}^3$ and $y_\omega \in \mathbb{R}^3$ are the accelerometer and gyroscope measurements, respectively, $b_a \in \mathbb{R}^3$ and $b_\omega \in \mathbb{R}^3$ represent the possible faults in accelerometer and gyroscope measurements, respectively. The terms d_a and d_ω represent the noise in the sensor measurements, and a represents the nominal acceleration measurement without bias, that is:

$$a = \frac{1}{m} \left(\begin{bmatrix} 0 \\ 0 \\ -U \end{bmatrix} - c_{\mathbf{d}} v_B \right) \tag{8}$$

The fault time profile functions $\beta_a(\cdot)$ and $\beta_\omega(\cdot)$ are assumed to be step functions with unknown fault occurrence times T_a and T_ω, respectively. Specifically,

$$\beta_a(t - T_a) = \begin{cases} 0\,, & \text{when } t < T_a \\ 1\,, & \text{when } t \geq T_a \end{cases}$$

$$\beta_\omega(t - T_\omega) = \begin{cases} 0\,, & \text{when } t < T_\omega \\ 1\,, & \text{when } t \geq T_\omega \end{cases}$$

In addition, it is assumed that the position measurements in the Earth frame available. Hence, the system model can be augmented by the following output equation:

$$y_p = p_E + d_p\,, \tag{9}$$

where d_p represents zero mean position measurement noise.

Assumption 1. The bias in accelerometer and gyroscope measurements are assumed to be constant and bounded.

Remark . It is worth noting that, in practical applications, after the occurrence of an IMU sensor bias, its magnitude may be time-varying and grow slowly over time. However, the change in the bias is often small over a short time duration. Therefore, the bias may be assumed to be constant during the short time duration under consideration.

Assumption 2. The sensor measurement noise signals denoted by d_a, d_ω and d_p are assumed to be bounded zero mean signals. That is:

$$\mathbb{E}(d_a) = 0, \qquad \mathbb{E}(d_\omega) = 0, \qquad \mathbb{E}(d_x) = 0,$$

where $\mathbb{E}$ represents the expectation operator.

The objective of this research focuses on the development and demonstration of a robust fault detection, isolation and estimation scheme for sensor faults in accelerometer and gyroscope measurements.

3. FAULT DETECTION AND ISOLATION

This section presents the proposed method for detecting and isolating sensor faults in accelerometer and gyroscope measurements. Substituting the sensor model given by Eq (6)-(7) into the systems dynamics Eq (1)-(4), we obtain:

$$\dot{p}_E = v_E \tag{10}$$

$$\dot{v}_E = R_{EB}(\eta)y_a + \begin{bmatrix}0\\0\\g\end{bmatrix} - R_{EB}(\eta)\beta_a b_a - R_{EB}d_a \tag{11}$$

$$\dot{\eta} = R_\eta(\phi,\theta)y_\omega - R_\eta(\phi,\theta)\beta_\omega b_\omega - R_\eta(\phi,\theta)d_\omega \tag{12}$$

$$\dot{\omega} = \begin{bmatrix}\frac{J_y-J_z}{J_x}(y_q-\beta_\omega b_q-d_q)(y_r-\beta_\omega b_r-d_r)\\ \frac{J_z-J_x}{J_y}(y_r-\beta_\omega b_r-d_r)(y_p-\beta_\omega b_p-d_p)\\ \frac{J_x-J_y}{J_z}(y_p-\beta_\omega b_p-d_p)(y_q-\beta_\omega b_q-d_q)\end{bmatrix} + \begin{bmatrix}\frac{1}{J_x}\tau_\phi\\ \frac{1}{J_y}\tau_\theta\\ \frac{1}{J_z}\tau_\psi\end{bmatrix} \tag{13}$$

where $R_\eta(\phi,\theta)$ is the rotation matrix relating angular rates to Euler angle rates and is given by:

$$R_\eta(\phi,\theta) = \begin{bmatrix}1 & \sin\phi\tan\theta & \cos\phi\tan\theta\\ 0 & \cos\phi & -\sin\phi\\ 0 & \sin\phi\sec\theta & \cos\phi\sec\theta\end{bmatrix}.$$

As can be seen from Eq (10)-(13), a bias in accelerometer measurements affects only the position and velocity states. Conversely, gyroscope measurements affect only Euler angles and angular rates states. Based on this observation, it follows naturally to also divide the fault diagnosis of these two sensor faults. The proposed fault detection, isolation and estimation architecture is shown in Figure 1. As can be seen, two FDI estimators monitor the system for fault occurrences in accelerometer and gyroscope measurements. Once a fault is detected and isolated, the corresponding nonlinear adaptive estimator is activated for sensor bias estimation purposes.

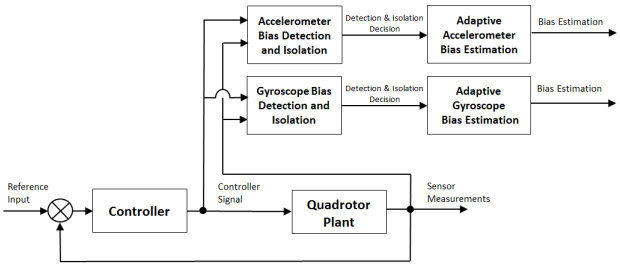

Figure 1. Fault detection, isolation and estimation architecture.

3.1. Gyroscope Fault Diagnostic Estimator

As can be seen from the dynamics of the quadrotor, given by equations (10)-(13), the bias in the gyroscope measurements only affects the attitude and rotation dynamics given by Eq (12)-(13). Based on Eq (12) and adaptive estimation schemes (Ioannou & Sun, 1996), the fault diagnostic estimator for the gyroscope bias can be designed as follows:

$$\dot{\hat{\eta}} = -\Lambda(\hat{\eta}-\eta) + R_\eta(\phi,\theta)y_\omega\,, \tag{14}$$

where $\hat{\eta} \in \mathbb{R}^3$ are the Euler angle estimates, $\Lambda \in \mathbb{R}^{3\times3}$ is a positive-definite diagonal design matrix. Let the Euler angle estimation error be defined as:

$$\tilde{\eta} \triangleq \eta - \hat{\eta}\,. \tag{15}$$

Based on Eq (12) and Eq (14), the dynamics of the attitude angle estimation error are given by:

$$\dot{\tilde{\eta}} = \dot{\eta} - \dot{\hat{\eta}} = -\Lambda\tilde{\eta} - R_\eta(\phi,\theta)\beta_\omega b_\omega - R_\eta(\phi,\theta)d_\omega\,. \tag{16}$$

By design, the homogeneous part of Eq (16) is exponentially stable. In the absence of a gyroscope fault (i.e. $t < T_0$), the attitude angle estimation error is given by:

$$\begin{aligned}\tilde{\eta}(t) &= e^{-\Lambda(t-T_0)}\tilde{\eta}(0) - \int_0^t e^{-\Lambda(t-\tau)}R_\eta(\phi,\theta)d_\omega d\tau\\ &= r_\omega(t) + e_\omega(t)\,,\end{aligned} \tag{17}$$

where $r_\omega(t) \triangleq e^{-\Lambda(t-T_0)}\tilde{\eta}(0)$ converges exponentially fast to zero, and $e_\omega(t)$ represents an additive noise term generated by filtering the measurement noise d_ω through the following linear filter:

$$\dot{e}_\omega = -\Lambda e_\omega - R_\eta(\phi,\theta)d_\omega$$

In addition, in the presence of a non-zero bias b_ω, based on Eq (16), it can be seen that the residual $\tilde{\eta}$ will deviate from zero. Therefore, if any component of the state estimation error $\tilde{\eta}$ is significantly different from zero, we can conclude that a fault in the gyroscope measurements has occurred.

3.2. Accelerometer Fault Diagnostic Estimator

The dynamics of UAV position and velocity relative to the inertial frame given by Eq (10) and Eq (11) can be represented by the following state space model:

$$\begin{aligned} \dot{x} &= Ax + f(\eta, y_a) + G_a(\eta)\beta_a b_a + D_a(\eta, t) \\ y &= Cx + d_p \,, \end{aligned} \tag{18}$$

where $x = [p_E^T \; v_E^T]^T$, $y = p_E$, and

$$A = \begin{bmatrix} 0_{3\times3} & I_3 \\ 0_{3\times3} & 0_{3\times3} \end{bmatrix}, \quad G_a(\eta) = \begin{bmatrix} 0_{3\times3} \\ -R_{EB} \end{bmatrix},$$

$$f(\eta, y_a) = \begin{bmatrix} 0_{3\times1} \\ R_{EB}y_a + \begin{bmatrix} 0 \\ 0 \\ g \end{bmatrix} \end{bmatrix}, \quad D_a(\eta, t) = \begin{bmatrix} 0_{3\times1} \\ -R_{EB}d_a \end{bmatrix},$$

and $C = [I_3, \; 0_{3\times3}]$, where I_3 is a 3×3 identity matrix, $0_{3\times3}$ is a 3×3 matrix with all entries zero and $0_{3\times1}$ is a 3×1 zero vector. Based on this configuration, the following fault diagnostic observer is chosen :

$$\begin{aligned} \dot{\hat{x}} &= A\hat{x} + f(\eta, y_a) + L(y - \hat{y}) \\ \hat{y} &= C\hat{x} \,, \end{aligned} \tag{19}$$

where $\hat{x} \in \mathbb{R}^6$ represents the inertial position and velocity estimation, $\hat{y} \in \mathbb{R}^3$ are the predicted position outputs, L is a design matrix chosen such that the matrix $\bar{A} \triangleq (A - LC)$ is stable. Let us define the position estimation error and the state estimation error as:

$$\tilde{y} \triangleq y - \hat{y} \tag{20}$$

$$\tilde{x} \triangleq x - \hat{x} \,. \tag{21}$$

By using equations (18) - (19), the estimation error dynamics are given by:

$$\begin{aligned} \dot{\tilde{x}} &= \bar{A}\tilde{x} + G_a(\eta)\beta_a b_a + D_a(\eta, t) - Ld_p \\ \tilde{y} &= C\tilde{x} + d_p \end{aligned} \tag{22}$$

In the absence of accelerometer bias, the position estimation error is given by:

$$\begin{aligned} \tilde{y} &= Ce^{\bar{A}(t-T_0)}\tilde{x}(0) + C\int_0^t e^{\bar{A}(t-\tau)}(D_a(\eta,t) - Ld_p)d\tau + d_p \\ &= r_a(t) + e_a(t) + d_p, \end{aligned} \tag{23}$$

where $r_a(t) \triangleq Ce^{\bar{A}(t-T_0)}\tilde{x}(0)$ converges exponentially fast to zero, and $e_a(t)$ represents an additive noise term generated by filtering d_a and d_p through the following linear filter:

$$\dot{e}_a = \bar{A}e_a + \Big(D_a(\eta,t) - Ld_p\Big).$$

Clearly, the output estimation error $\tilde{y}$ reaches a small value, centered around zero, exponentially fast in the absence of the accelerometer bias b_a. Furthermore it can be seen from Eq (22) the residual $\tilde{y}$ is only sensitive to the bias b_a. Therefore, if any component of the position estimation error $\tilde{y}$ deviates significantly from zero, we can conclude that a fault in the accelerometer sensor measurement has occurred.

3.3. Fault Detection and Isolation Decision Scheme

As described in Section 3.1 and 3.2, the two fault diagnostic estimators are designed such that each of them is only sensitive to one type of sensor faults. Based on this observation, the residuals $\tilde{\eta}$ and $\tilde{y}$ generated by Eq (17) and Eq (23) can also be used as structured residuals for fault isolation. More specifically, we have the following fault detection and isolation decision scheme:

- In the absence of any faults, all components of the residuals $\tilde{\eta}$ and $\tilde{y}$ should be close to zero.
- If all components of the residual $\tilde{\eta}$ remain around zero, and at least one component of the residual $\tilde{y}$ is significantly different from zero, then we conclude that an accelerometer fault has occurred.
- If all components of the residual $\tilde{y}$ remain around zero, and at least one component of the residual $\tilde{\eta}$ is significantly different from zero, then we conclude that a gyroscope fault has occurred.
- If at least one component of the residual $\tilde{\eta}$ and at least one component of the residuals $\tilde{y}$ are simultaneously significantly different from zero, then we conclude that both a gyroscope and accelerometer sensor measurement fault has occurred.

The above FDI decision scheme is summarized in Table 1, where "0" represents residuals with zero mean, and "1" represents significantly non-zero residuals.

Table 1. Fault Isolation Decision Truth Table.

	No Fault	Gyro Bias	Accel Bias	Accel & Gyro Bias
$\tilde{\eta}$	0	1	0	1
$\tilde{y}$	0	0	1	1

4. FAULT ESTIMATION

After a sensor fault is detected and isolated, it is also crucial to provide an estimation of the sensor bias to improve the performance of the closed loop control system. As shown in Figure 1, once a fault has been detected and isolated, the corresponding nonlinear adaptive bias estimator is activated with the purpose of estimating the fault magnitude in the accelerometer and/or gyroscope measurements. In this section, we describe the design of nonlinear adaptive estimators for sensor bias estimation.

4.1. Accelerometer Fault Estimation

Based on Eq (18), the adaptive observer for estimating the accelerometer bias magnitude is chosen as:

$$\dot{\hat{x}} = A\hat{x} + f(\eta, y_a) + L(y - \hat{y}) + G_a(\eta)\hat{b}_a + \Omega\dot{\hat{b}}_a \quad (24)$$

$$\dot{\Omega} = (A - LC)\Omega + G_a(\eta) \quad (25)$$

$$\hat{y} = C\hat{x}\,, \quad (26)$$

where $\hat{x}$ is the estimated position and velocity vector, $\hat{y}$ is the estimated position output, $\hat{b}_a$ is the estimated sensor bias, and L is the observer gain matrix. The adaptation in the above adaptive estimator arises due to the unknown bias b_a. The adaptive law for updating $\hat{b}_a$ is derived using Lyapunov synthesis approach (Bastin & Gevers, 1988; Zhang, 2011) and is given by:

$$\dot{\hat{b}}_a = \mathcal{P}_\Theta\{\Gamma\Omega^T C^T\tilde{y}\}. \quad (27)$$

In order to guarantee the stability of the parameter estimation in the presence of unknown modeling errors and measurement noise (Ioannou & Sun, 1996), the projection operator $\mathcal{P}$ restricts the parameter estimate to a known compact convex region Θ, defined by $\hat{b}_a^T\hat{b}_a < M^2$, where M is a positive constant. Specifically, the adaptive algorithm is given by:

$$\dot{\hat{b}}_a = \begin{cases} \Gamma\Omega^T C^T\tilde{y}, & \text{if } ||\hat{b}_a|| = M \text{ and } \hat{b}_a^T\Gamma\Omega^T C^T\tilde{y} \le 0 \\ & \text{or if } ||\hat{b}_a|| < M \\ \Gamma\Omega^T C^T\tilde{y} - \Gamma\frac{\hat{b}_a\hat{b}_a^T}{\hat{b}_a^T\Gamma\hat{b}_a}\Gamma\Omega^T C^T\tilde{y}, & \text{otherwise} \end{cases} \quad (28)$$

where $\Gamma > 0$ is a symmetric and positive-definite learning rate matrix, and $\tilde{y}_a \triangleq y_a - \hat{y}_a$ is the output estimation error. Let us also define the state estimation error as $\tilde{x} \triangleq x - \hat{x}$, and the parameter estimation error as $\tilde{b}_a \triangleq \hat{b}_a - b_a$. The stability and performance properties of the above adaptive scheme are described below.

Theorem 4.1. In the presence of an accelerometer measurement bias, if there exists constants $\alpha_1 \ge \alpha_0 > 0$ and $T_0 > 0$, such that

$$\alpha_1 I \ge \frac{1}{T_0}\int_t^{t+T_0} \Omega^T C^T C\Omega d\tau \ge \alpha_0 I\,, \quad (29)$$

then, the adaptive scheme described by Eq (24) - (26) and Eq (28) ensures that:

1. all signals in the adaptive estimator remain bounded,
2. $\mathbb{E}(\tilde{x})$ and $\mathbb{E}(\tilde{b}_a)$ converge exponentially to zero.

The proof of the above theorem is omitted here due to space limitation. Interested readers please contact the corresponding author for details (Avram, 2015).

4.2. Gyroscope Fault Estimation

Once a gyroscope bias fault is detected and isolated, the following adaptive estimator is activated in order to estimate the bias in the gyroscope sensor:

$$\dot{\hat{\eta}} = -\Lambda(\hat{\eta} - \eta) + R_\eta(\phi,\theta)y_\omega - R_\eta(\phi,\theta)\hat{b}_\omega \quad (30)$$

$$\dot{\hat{b}}_\omega = \Gamma R_\eta(\phi,\theta)(\hat{\eta} - \eta)\,, \quad (31)$$

where $\hat{\eta}$ is the Euler angle estimate, $\hat{b}_\omega$ represents the estimation of the sensor bias, Λ and Γ are positive definite design matrices. The adaptive law for estimating the bias in gyroscope measurements in Eq (30)- (31) is derived using Lyapunov synthesis approach (Ioannou & Sun, 1996). In addition, in order to ensure parameter convergence, $R_\eta(\phi,\theta)$ will also need to satisfy the persistence of excitation condition (Ioannou & Sun, 1996), that is:

$$\alpha_1 I \ge \frac{1}{T_0}\int_t^{t+T_0} R_\eta(\phi,\theta)^T R_\eta(\phi,\theta)d\tau \ge \alpha_0 I \quad (32)$$

for some constants $\alpha_1 \ge \alpha_0 > 0$ and $T_0 > 0$ and for all $t \ge 0$. Let us define the attitude angle estimation error as $\tilde{\eta} \triangleq \eta - \hat{\eta}$ and the bias estimation error as $\tilde{b}_\omega \triangleq \hat{b}_\omega - b_\omega$. The stability and learning performance of the adaptive scheme Eq (30)- (31) is summarized by the following theorem.

Theorem 4.2. In the presence of a gyroscope bias, if there exists constants $\alpha_1 \ge \alpha_0 > 0$ and $T_0 > 0$ such that Eq (32) is satisfied, then the adaptive scheme in Eq (30) - (31) ensures that:

1. all signals in the adaptive scheme remain bounded
2. $\mathbb{E}(\tilde{\eta})$ and $\mathbb{E}(\tilde{b}_\omega)$ converge exponentially to zero.

For the sake of space limitation, the complete proof of the above theorem is purposely omitted. Interested readers please contact the corresponding author for details (Avram, 2015).

5. EXPERIMENTAL RESULTS

In this section, experimental results using a real-time quadrotor test environment of Wright State University are described to illustrate the effectiveness of the sensor fault diagnosis algorithm. A block diagram of the experimental system setup is shown in Figure 2. During flight tests, quadrotor position and attitude information is obtained from a Vicon motion capture camera system. Position and Euler angle measurements are collected every 10ms and relayed from a Vicon dedicated PC via TCP/IP connection to a ground station computer. As in (Macdonald, Leishman, Beard, & McLain, 2014), we corrupted position measurements with normal noise. In this research we chose the noise standard deviation to be 0.25m. Additionally, position measurements are down sampled to 1Hz, in order to further simulate real world applications. The fault diagnosis method is evaluated in real-time during autonomous flight of a quadrotor built in-house with off-the-shelf components. The quadrotor is equipped with the Qbrain embedded control module from Quanser Inc. The control module consists of a HiQ acquisition card providing real-time IMU measurements, and a Gumstix Duo Vero micro-

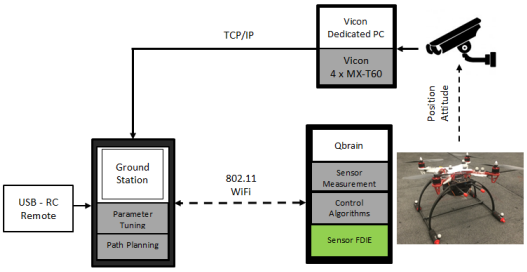

Figure 2. Experimental system architecture setup

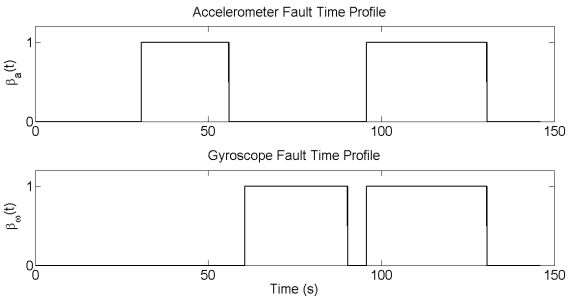

Figure 3. Sensor fault time profile

controller running the real-time control software. An IEEE 802.11 connection between the ground station PC and the Gumstix allows for fast and reliable wireless data transmission and on-line parameter tuning. Position and attitude information obtained from the Vicon system along with trajectory commands generated by the ground station are sent to the quadrotor in order to achieve real-time autonomous flight. The control software executes on-board at 500Hz, and accelerometer and gyroscope measurement are logged at 200Hz. During the experimental stage, the quadrotor is commanded to move in a circular trajectory, while maintaining constant orientation and altitude. As previously shown, the fault diagnosis technique employed in this approach is independent of the structure of the controller. Therefore, for brevity, the discussion on the control design is purposely omitted.

In order to evaluate the proposed diagnosis method, we log approximately 2.5 minutes of autonomous flight data. Sensor bias is artificially injected into the accelerometer and gyroscope measurements, respectively, while the quadrotor is airborne. Figure 3 shows the fault time profile of the two sensor faults. As can be seen, an accelerometer fault is injected approximately at time $t = 35s$ until $t = 60s$. From approximately $t = 62s$ until $t = 95s$, a gyroscope bias is introduced into the sensor measurements. Additionally, in order to evaluate the performance of the proposed FDIE algorithm in the presence of multiple faults, both accelerometer and gyroscope faults are injected at approximately $t = 97s$. Flight data is processed on-line, and real-time sensor fault diagnostic decision is provided by the diagnostic algorithm. In the following sections, we present the evaluation results of the diagnosis method using real-time flight data.

5.1. Case of Accelerometer Bias

The performance of the proposed FDIE in the presence of accelerometer measurement bias fault is shown in this section. At approximately time $t = 35s$, a constant bias $b_a = [0.1,\ 0.15,\ 0.9]^T m/s^2$, is injected into the accelerometer measurements. Figure 4 shows the residuals generated by the two diagnostic estimators described by Eq (14) and Eq (19), respectively. In order to enhance the diagnostic decision based on the FDI logic given by Table 1, the two-sided cumulative sum (CUSUM) test is applied to process the diagnostic residuals (Gustafsson, 2000). Figure 5 shows the statistic property generated by the CUSUM test. A fixed threshold is chosen for the detection and isolation of sensor faults. As can be seen, shortly after the occurrence of the fault, at least one component of the test statistic corresponding to the residuals generated by the accelerometer diagnostic estimator exceeds the detection threshold. On the other hand, all components of the test statistic corresponding to the gyroscope bias remain well below the detection threshold. Based on the detection and isolation logic given in Table 1, we can conclude that a fault has occurred in the accelerometer measurement. In addition, Figure 6 shows the estimation of the bias in the accelerometer for each axis, respectively. As can be seen, the estimate of accelerometer converges closely to the actual value.

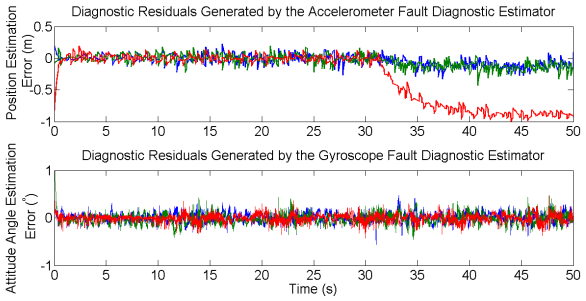

Figure 4. Sensor bias diagnostic raw residuals.

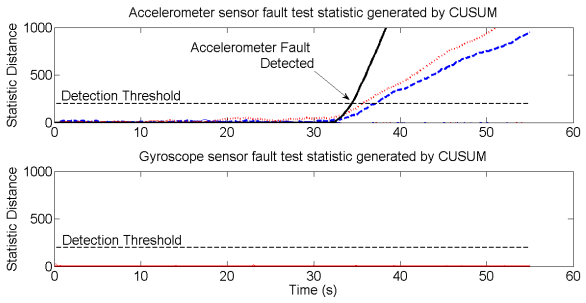

Figure 5. Accelerometer fault diagnosis using CUSUM.

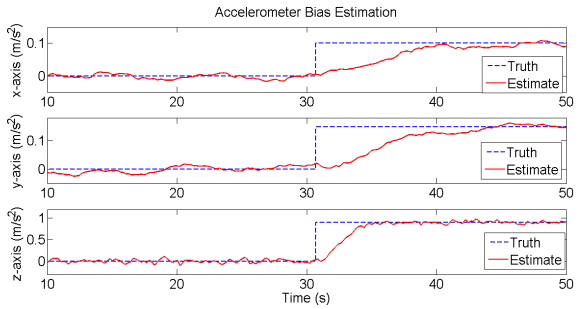

Figure 6. Accelerometer bias estimation.

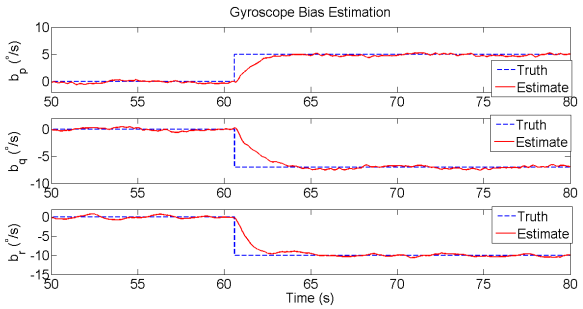

Figure 8. Gyroscope bias estimation.

5.2. Case of Gyroscope Bias

A gyroscope bias with $b_\omega = [5,\ -7,\ -10]^T{}^\circ/s$ is injected into the sensor measurements at approximately time $t = 62s$. Figure 7 shows the statistic property generated by the CUSUM test when applied to the residuals generated by Eq (14) and Eq (19), respectively. As can be seen, at least one component of the test statistic corresponding to the residuals generated by the gyroscope diagnostic estimator exceeds the manual chosen detection threshold shortly after the occurrence of the gyroscope fault. On the other hand, all components of the test statistic corresponding to the accelerometer bias remain well below the detection threshold. Based on the detection and isolation logic given in Table 1, we can conclude that a fault has occurred in the gyroscope measurement. In addition, Figure 8 shows the estimation of the bias in the gyroscope for each axis, respectively. As can be seen, after a short time, the estimate of gyroscope bias is reasonably close to its actual value.

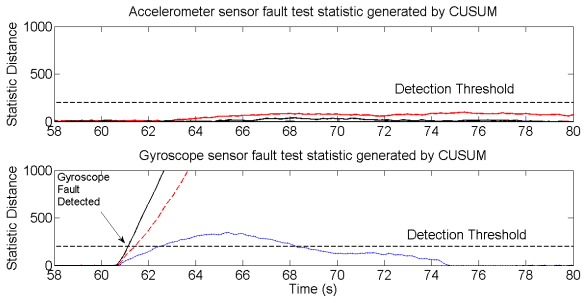

Figure 7. Gyroscope fault diagnosis using CUSUM.

5.3. Case of Simultaneous Faults

In this section, we present the results of the diagnostic method in the presence of both accelerometer and gyroscope faults. Specifically, at time $t = 97s$, biases $b_a = [0.1,\ 0.15,\ 0.9]^T m/s^2$ and $b_\omega = [5,\ -7,\ -10]^T\ {}^\circ/s$ are injected into accelerometer and gyroscope measurements, respectively. Figure 9 shows the statistic property generated by the CUSUM test. As can be seen, shortly after the occurrence of the faults, the test statistics corresponding to both diagnostic estimators, exceed their respective detection threshold. Hence, we can conclude that faults have occurred in both accelerometer and gyroscope measurements. Furthermore, Figure 10 and Figure 11 show the estimation of the accelerometer and gyroscope biases, respectively. As can be seen, estimation results are satisfactory.

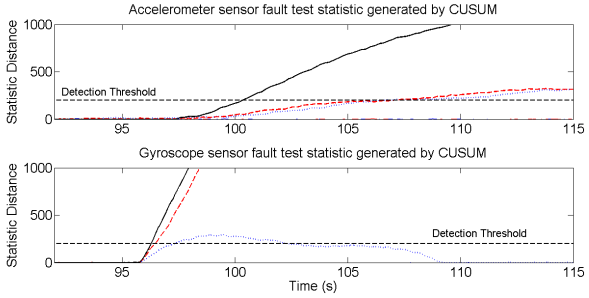

Figure 9. CUSUM based fault detection of simultaneous sensor faults.

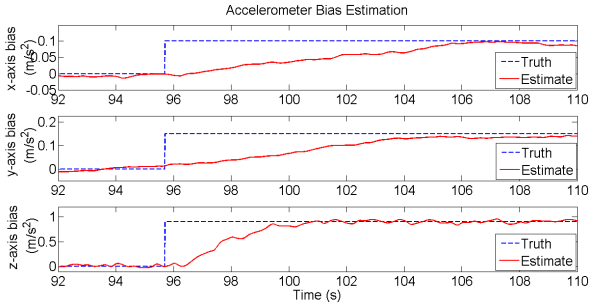

Figure 10. Accelerometer bias estimation in the simultaneous fault occurrence scenario.

6. CONCLUSION AND FUTURE WORK

In this paper, we present the design of a nonlinear fault diagnostic method for sensor bias faults in accelerometer and gyroscope measurements of quadrotor UAVs. Based on the idea that accelerometer and gyroscope measurements coincide with translational and rotational forces acting on the body, respectively, two FDI estimators are designed to generate structured residuals for fault detection and isolation. In addition,

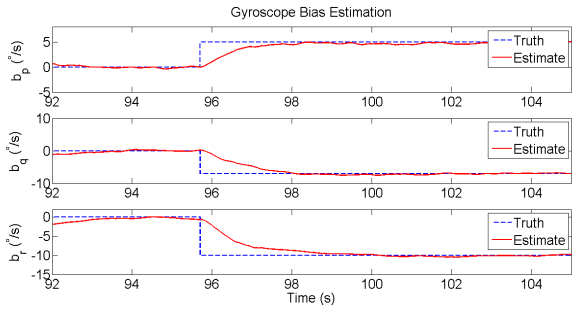

Figure 11. Gyroscope bias estimation in the simultaneous fault occurrence scenario.

nonlinear adaptive estimation estimation schemes are presented to provide an estimate of the sensor bias. The proposed diagnostic method is implemented on a quadrotor UAV test environment and is demonstrated during real-time autonomous flight data. An interesting direction for future research is to develop and demonstrate a systematic diagnostic method for quadrotor actuator faults.

REFERENCES

Avram, R. C. (2015). *Fault Diagnosis and Fault Tolerant Control of Quadrotor UAVs* (Tech. Rep.). Wright State University, Dayton, OH.

Bastin, G., & Gevers, M. (1988, Jul). Stable adaptive observers for nonlinear time-varying systems. *IEEE Transactions on Automatic Control*, *33*(7), 650-658.

Guenard, N., Hamel, T., & Mahony, R. (2008). A practical visual servo control for an unmanned aerial vehicle. *IEEE Transaction on Robotics*, *24*(2).

Gustafsson, F. (2000). *Adaptive filtering and change detection*. Wiley, West Sussex, England.

Ioannou, P. A., & Sun, J. (1996). *Robust Adaptive Control*. Mineola, New York: Dover Publications, Inc.

Ireland, M., & Anderson, D. (2012). Development of navigation algorithms for NAP-of-the-earth UAV flight in a constrained urban environment. In *28th International Congress of the Aeronautical Sciences.*

Lantos, B., & Marton, L. (2011). *Nonlinear Control of Vehicles and Robots*. Springer-London.

Leishman, R. C., Jr., J. C. M., Beard, R. W., & McLain, T. (2014). Quadrotors and accelerometers. State estimation with an improved dynamic model. *IEEE Control Systems Magazine*, *34*(1).

Macdonald, J., Leishman, R., Beard, R., & McLain, T. (2014). Analysis of an improved IMU-based observer for multirotor helicopters. *Journal of Intelligent Robotic Systems*, *64*, 1049-1061.

Martin, P., & Salaün, E. (2010). The true role of accelerometer feedback in quadrotor control. In *IEEE International Conference on Robotics and Automtation.*

Shima, T., & Rasmussen, S. (2008). UAV cooperative decision and control: Challenges and practical approaches. In *SIAM.*

Zhang, X. (2011). Sensor bias fault detection and isolation in a class of nonlinear uncertain systems using adaptive estimation. *IEEE Transaction on Automatic Control*, *56*(5).

Zhang, X., Polycarpou, M., & Parsini, T. (2001). Robust fault isolation for a class of non-linear input-output systems. *International Journal Control*, *74*(13).

BIOGRAPHIES

Remus C. Avram is a PhD candidate at Wright State Univerisity, Dayton OH. Remus, received his B.S. in Electrical Engineering with concetration in Computer Engineering at University of Texas, San Antonio, Texas in 2009. In 2011, Remus obtained his M.S. in Electrical Engineering with concetration in Control Systems from Wright State University, Dayton, Ohio. He is currently pursuing a doctoral degree in Electrical Engineering. Remus's main research include nonlinear health diagnostic methods and real-time intelligent control.

Xiaodong Zhang received the B.S. degree from Huazhong University of Science and Technology, Wuhan, China, the M.S. degree from Shanghai Jiao Tong University, Shanghai, China, and the Ph.D. degree from University of Cincinnati, Cincinnati, OH, USA, all in electrical engineering, in 1994, 1997 and 2001, respectively. He is currently an Associate Professor of Electrical Engineering Department, Wright State University, Dayton, OH. His research interests include intelligent control systems, fault diagnosis and prognosis, fault-tolerant control, verification and validation of control systems for safety assurance, etc. He is an Associate Editor of the IEEE Transactions on Control Systems Technology and a member of the IFAC SAFEPROCESS Technical Committee.

Jonathan Muse received an undergraduate degree from the University of Alabama in 2005, a Masters Degree from the Georgia Institute of Technology in 2008, and a PhD in Aerospace Engineering from the Georgia Institute of Technology in 2010. He is currently a research engineer for the Aerospace Systems Directorate at the Air Force Research Lab (AFRL). At AFRL, he is responsible for executing basic research related to hypersonic vehicle control and advanced methods in nonlinear control. He is the Co-PI for HIFiRE flight 6, an adaptive flight control experiment on a scramjet hypersonic vehicle currently being constructed. He also holds an adjunct professor position at Wright State University in the Electrical Engineering department where he teaches control theory and UAV flight control. In addition, he also serves on various advisory boards for both industry and academia.